Colloids and Surfaces B: Biointerfaces 134 (2015) 131–139

Contents lists available at ScienceDirect

Colloids and Surfaces B: Biointerfaces

journal homepage: www.elsevier.com/locate/colsurfb

Application of the Johnson–Kendall–Roberts model in AFM-based mechanical measurements on cells and gel.

Yu.M. Efremov*, D.V. Bagrov, M.P. Kirpichnikov, K.V. Shaitan

Lomonosov Moscow State University, Faculty of Biology, Leninskie Gory 1/73, Moscow 119234, Russia

ARTICLE INFO

Article history:
Received 27 March 2015
Received in revised form 2 June 2015
Accepted 22 June 2015
Available online 26 June 2015

Keywords:
Force spectroscopy
Mechanical properties
Adhesion
Viscoelasticity
Cell
Polyacrylamide gel

ABSTRACT

The force-distance curves (FCs) obtained by the atomic force microscope (AFM) with colloid probes contain information about both the viscoelastic properties and adhesion of a sample. Here, we processed both the approach and retraction parts of FCs obtained on polyacrylamide gels (in water or PBS) and Vero cells (in a culture medium). The Johnson–Kendall–Roberts model was applied to the retraction curves to account for the adhesion. The effects of loading rate, holding time and indentation depth on adhesion force and Young's modulus, calculated from approach and retraction curves, were studied. It was shown that both bulk and local interfacial viscoelasticity can affect the observed approach-retraction hysteresis and measured parameters. The addition of 1% bovine serum albumin (BSA) decreased adhesion of the probe to the PAA gel surface, so interfacial viscoelasticity effects were diminished. On the contrary, the adhesiveness of Vero cells increased after BSA addition, indicating the complex nature of the cell-probe interaction.

© 2015 Elsevier B.V. All rights reserved.

1. Introduction

Atomic force microscopy (AFM) has become a powerful tool for the analysis of mechanical properties of polymer samples and biological objects such as cells and tissues [1–6]. One of the key advantages of AFM is the ability to measure forces on the order of ten piconewtons under near physiological conditions. Typically, the mechanical properties of samples are evaluated during force spectroscopy experiments: the AFM probe first approaches the sample and indents it, then retracts; the force acting on the cantilever is recorded during this cycle. The obtained dependencies are called force versus distance curves (force curves, FCs). The colloidal probes, which consist of a spherical colloidal particle of few micrometers in diameter attached to an AFM cantilever, provide accurate control of the probe geometry [5,7–9]. Commonly the Hertz model or its modifications is applied to the approach (loading, extension) part of FCs to extract Young's modulus (E), the elastic parameter used for the characterization of the sample's mechanical properties.

AFM was used to quantify the Young's modulus of various animal cell types with colloidal probes and regular cantilevers [4,10–12]. These studies have demonstrated the link between cell mechanics and cytoskeleton structure, and found that cell mechanical properties altered in various diseases [1,13–15]. However, in most research the capabilities of force spectroscopy are not fully used. Retraction (unloading) curves containing information about adhesion and tether extraction are rarely evaluated [16,17], or only the adhesion region is analyzed [18,19]. Furthermore, the hysteresis observed in approach and retraction curves and attributed to the energy dissipation during indentation can be used for the estimation of cell viscoelastic properties (e.g. relaxation behavior) [15,20–22]. However, for the accurate determination of the stress relaxation from a whole AFM force–distance curve, both the contribution of the adhesion and the functional form of the relaxation must be assumed. These parameters can provide a deep insight into cell biomechanics and can be used as additional diagnostic markers.

Here, we address one of the key steps in whole AFM force–distance curve processing—the assessment of the adhesion contribution. Particularly, we try to answer several questions. First, what is the relation between the Young's moduli calculated from the approach and retraction parts of the force curve? Second, is there any connection between the adhesion force and the Young's modulus? Third, how could we process the force curves obtained at different indentation speeds to assess the viscoelastic properties of the samples? To answer these questions, we applied the JKR model to the retraction curves under different loading rates, holding times (delay between the sample indentation and probe retraction) and

* Corresponding author at: Leninskie Gory 1/73, Moscow, 119234, Russia. Fax: +7 4959395738.
E-mail address: yu.efremov@gmail.com (Yu.M. Efremov).

http://dx.doi.org/10.1016/j.colsurfb.2015.06.044
0927-7765/© 2015 Elsevier B.V. All rights reserved.

indentation depths (loading forces). Although both the Hertz and the JKR models assume the purely elastic nature of the sample, a comparison of Young's modulus and several additional parameters extracted from both approach and retraction curves can be used for the assessment of viscoelastic effects. Polyacrylamide hydrogels (PAA gels) and mammalian Vero cells were used as model samples. On the PAA gel samples, the addition of 1% BSA to the experimental medium decreased interfacial forces and allowed us to obtain data almost unaffected by adhesion.

2. Material and methods

2.1. Gel preparation

Solutions of acrylamide and bis-acrylamide (both 99% purity, Amresco, USA) in Milli-Q water or PBS (Amresco, USA) were polymerized with 10% ammonium persulfate (Sigma) and TEMED (Fluka, Germany). Concentrations of acrylamide (4%) and bis-acrylamide (0.1%, w/v) were chosen to prepare a PAA gel with approximately 1–2 kPa Young's modulus (E), which is in the range of eukaryotic cell compliances. The Young's modulus of the PAA gels in PBS was quantified by a rotational rheometer MCR 502 (Anton Paar GmbH, Graz, Austria) with plate–plate geometry. The equation $E=(1+2\nu)G$ was used, where $\nu=0.48$ is the Poisson's ratio of the PAA gel [23] and G is the measured shear modulus. For AFM experiments, a total solution volume of 100 μL was allowed to polymerize between 18 mm (top) and 24 mm (bottom) clean glass square coverslips (Menzel–Gläser, Germany). Then the top coverslip was removed and the sample was extensively washed with MQ water or PBS. Prepared PAA gels had thickness near 200 μm. For the rheometric measurements, PAA gel samples had 1 mm thickness. They were also prepared between two glass coverslips but the side face of the gel was closed by plasticine to maintain the sample thickness. The PAA gels were kept in PBS/water for several days before the experiments to reach equilibrium.

2.2. Cell culture

Vero cells were grown in a DMEM medium (PanEco, Russia) supplemented with 10% fetal bovine serum (FBS) (PAA Laboratories, Austria) at 37 °C in a humidified 5% CO_2 atmosphere in an incubator (Sanyo, Japan). Cells, subjected to AFM experiments, were seeded on sterile glass coverslips (Menzel–Gläser, Germany) and grown to about 60% confluency. Experiments were conducted at 37 °C after the growth medium was replaced with the L-15 medium (Leibovitz's L-15 Medium with L-glutamine, Gibco, Invitrogen) without FBS. Cells which were spread out and well-attached to the surface were chosen for the force spectroscopy. Force curves were taken at the central part of cells, where the cell height is large enough to minimize substrate effects [5]. Bovine serum albumin (BSA) was purchased from Amresco, USA.

2.3. AFM force spectroscopy

AFM measurements were performed using a commercial Solver Bio atomic force microscope (NT-MDT, Russia), combined with an inverted optical microscope (Olympus, Japan), as described previously [24]. This microscope is equipped with the closed-loop feedback system that corrects the piezo hysteresis and nonlinearities at a large displacement scale. Tipless AFM cantilevers CSG11 (NT-MDT, Russia) modified with 5–7 μm diameter silica glass beads (Sigma–Aldrich Co., USA) were used. The glass bead was glued to the end of the cantilever using two component epoxy glue (No 908, Dynatron/Bondo Corp., USA) under the control of the inverted optical microscope. The typical spring constant of these cantilevers is 0.03 N/m. The accurate value was determined using the thermal noise [25] and Sader methods [26]. The radius of the probe was calculated after scanning the test grating TGT1 (NT-MDT, Russia). Before experiments, the cantilevers were washed in toluene, ethanol and MQ water (15 min each). Before and after measurements, the relationship between the photodiode signal and cantilever deflection (sensitivity, S) was calibrated by recording several FCs at a bare region of the glass coverslip and measuring its slope. Typically, FCs were taken at 2 μm/s loading rate (piezo displacement speed along the Z axis), and the closed loop feedback was always used. The piezo displacement range was 5–10 μm (typically 8 μm) to obtain a non-contact region which is long enough and free from interactions with a surface (tethering). 50–60 cells in 5 samples (3 FCs per cell above its central part, where the cell is quite flat and their height is large enough to diminish substrate effects), and 3 PAA gel samples (10 FCs at 3 random locations for each sample) were analyzed. The holding time (residence time of the probe on the sample surface between approach and retraction with constant piezo displacement) was 0, 1, 5, and 10 s. In experiments with different loading rates, piezo displacement speed was between 0.27 and 32 μm/s. At a piezo speed of above 2 μm/s a hysteresis (separation) between approach and retraction in the contact part of calibration curves was detected, possibly caused by the inertial effects [27]. It linearly increased with the piezo speed and achieved 90 nm at 32 μm/s. The Δz_0 parameter was corrected for this effect.

2.4. FC processing

Adhesion force is neglected in the Hertz model, which is generally applicable to approach curves in AFM experiments. When the maximum adhesive (pull-off) force F_{ad} is large enough in comparison with the maximum force F_{max} applied during loading, i.e. for $|F_{ad}/F_{max}|>0.05$ [28], which is frequently observed in retraction curves, Hertzian analysis is no longer valid and models for adhesive contact of spheres should be invoked. These models include the JKR (Johnson–Kendall–Roberts), DMT (Derjaguin–Muller–Toporov), and Maugis models [28–30]. The JKR theory is valid for compliant samples, large tip radii, and high adhesion forces, while the DMT theory is applicable to stiffer samples, small tip radii, and low adhesion forces. These models actually represent the two extreme cases in adhesive interactions, and the transition regime between these limits is described in the Maugis model. The dimensionless Tabor parameter $\mu=(R\gamma^2/E^2\epsilon^3)^{1/3}$ is used to choose the suitable model [31]. Here, R is the radius of curvature of the colloidal probe (the surface of the sample is considered to be flat; roughness effects are small due to sample compliance), γ is the Dupré's work of adhesion (surface energy per unit area), E is the Young's modulus of the sample (the sample is much softer than the material of the probe), and ϵ is the equilibrium separation between the surfaces (typically taken to be within a range 0.3–0.5 nm). Regions of applicability of the DMT and JKR models are defined by $\mu<0.1$, and $\mu>5$, respectively. For the typical experimental setup, we obtain the Tabor parameter of $\mu\approx200$, so the JKR model is preferred. The JKR model gives the following equations for the indentation depth δ, the contact radius a and the maximum adhesive force F_{ad}:

$$\delta=\frac{a^2}{R}-\frac{4}{3}\sqrt{\frac{aF_{ad}}{RK}}; \tag{1}$$

$$a=\left[\frac{R}{K}\left(\sqrt{Fa_d}+\sqrt{F+Fa_d}\right)^2\right]^{\frac{1}{2}}; \tag{2}$$

$$F_{ad}=\frac{3}{2}\pi\gamma R; \tag{3}$$

where $K = (4/3)E(1-\nu^2)$ is the elastic constant of the sample, and F is the normal loading force [29]. Like the Hertz model, the JKR model also assumes the sample as purely elastic.

Raw AFM indentation data are presented in the form of cantilever deflection d (units of nm, after the sensitivity value is applied to the signal from the photodiode) as a function of the piezo displacement z (units of nm), where the cantilever base is attached. The loading force was determined by multiplying the cantilever deflection by its spring constant on the basis of Hooke's law. The zero force (zero deflection, $d = 0$) level was calculated by the linear approximation of non-contact regions for the approach and retraction parts of FC independently, and then it was subtracted from them. Both indentation δ and cantilever deflection d occur during the piezo displacement z and $(z - z_0) = \delta + d$, so the reference point of zero indentation z_0 should be determined. In the approach curves (the Hertz model) this point coincides with the contact point, which was determined as described previously [24]. In the JKR model, assumed for the retraction curves, the nonzero contact radius a_{min} and negative indentation depth occur at maximum adhesion force F_{ad} just before separation of the probe and the sample (jump-out contact). According to the model, the zero indentation point corresponds to the point where $F = -0{,}89F_{ad}$. The JKR theory is applicable under thermodynamic equilibrium conditions only, so the loading data and the unloading data should follow the same path reversibly (although long-range force is required for jump-to-contact during approach). The computed FC following the JKR model is presented on Fig. 1A. Tensile ($F < 0$), and compressive ($F > 0$) regions and the special points are marked. On the experimental FCs (Fig. 1B–D), the approach and retraction parts are clearly distinguished while adhesion is observed only on retraction parts (except curves on the PAA gel in water on Fig. 1B). The tethering region is also frequently observed after F_{ad} point during retraction.

are proposed for the processing of adhesion-containing force curves with the JKR model [17]. Here, we used the measured values of d to calculate fitted values of z, as proposed by Lin et al. [17]:

$$z = z_0 + d + \frac{a^2}{R} - \frac{4}{3}\sqrt{\frac{aF_{ad}}{RK}} \quad (4)$$

where Eq (2) should be substituted for the contact radius a. The nonlinear least squares fitter (NLSF) of Origin 6 (OriginLab, MA) was used to fit the data. To decrease the number of iterations during fitting, the values of E and z_0 from the approach curve were used as initial guess; also the F_{ad} parameter was found before fitting as the local minimum on the retraction curve. To summarize, the following steps were implemented for the whole AFM force–distance curves processing:

- Identification of zero force level for both approach and retraction curves;
- determination of contact point z_{0app} in the approach curve, estimation of Young's modulus E_{app} by fitting the contact portion of the approach curve with the Hertz model (an exception was made for the PAA gels in water, as described below);
- determination of F_{ad} in the retraction curve, estimation of the zero indentation point z_{0retr} and Young's modulus E_{retr} by fitting the contact portion of the retraction curve with the JKR model;
- estimation of derivative parameters: the ratio E_{app}/E_{retr}, the difference between zero indentation points during approach and retraction $\Delta z_0 = z_{0retr} - z_{0app}$, the work of detachment (mechanical work required to detach the probe from the cell, which is obtained by integrating the area under the retraction curve restricted to the tensile region), and the force decay in experiments with the varying holding times. Some of these parameters provide a quality assessment of sample viscoelastic properties.

We observed instabilities in the tensile parts of some retraction curves on cells and gels (Fig. S1), so only the compressive part was used for fitting as proposed in [32]. It also seems that the upper part of retraction curves obtained on cells (high loading forces) is mostly affected by relaxation processes since it significantly deviates from the Hertz model (Fig. 1D). So, the first 500 or 750 nm of the indentation of approach curves and the corresponding part of retraction curves were used for the fitting procedure in experiments with Vero cells and PAA gels, respectively.

3. Results

3.1. PAA gels in water

The jump-to-contact phenomenon was observed in the approach part of FCs obtained on the PAA gels in MQ water (Fig. 1B). The attraction between the probe and the gel was observed in the approach curves at distances of 100–200 nm from the eventual snap-in (Fig. S2). Presumably, this is caused by a combination of electrostatic and van der Waals attractive forces. The pH of MQ water was ≈6 due to dissolved CO_2 and silica glass microspheres had a negative surface charge, primarily through the dissociation of terminal silanol groups [33]. The PAA gels should be electrically neutral because uncharged monomers are used. However, it seems in our experiments as if they had a moderate positive charge, possibly due to the presence of impurities in the reagents, so electrostatic attraction with the probe is arises. On the calibration curves obtained at the bare glass surface, which has a negative charge in water, the electrostatic repulsion was observed at the same distances 100–200 nm (Fig. S2).

The JKR model was applied both to approach and retraction curves, which displayed some hysteresis. The maximum adhesion force F_{ad} was ~50% larger on the retraction curves (1.2 ± 0.4 nN versus 0.8 ± 0.3 nN on approach curves). The distributions of E_{app} (1000 ± 60 Pa), E_{retr} (1000 ± 80 Pa), Δz_0 (90 ± 50 nm) and F_{ad} were close to normal (Figs. S3–S5), and the variability was low within the data obtained on the one PAA gel sample (coefficient of variation CoV ≈3%, 5%, 10% for E_{app}, E_{retr} and F_{ad}, respectively), but larger variability was found between the samples prepared on different days (CoV ≈6%, 8%, 30%). Some subtle uncontrolled experimental factors (temperature fluctuations, polymerization time and others) could affect the PAA gel mechanical properties.

The effects of loading rate on E_{app}, E_{retr}, F_{ad}, and Δz_0 were examined by varying the piezo speed for a constant maximum load F_{max} (≈9–10 nN). At the highest speed used (32 μm/s), the hydrodynamic force acting on the cantilever was observed as increased separation between the non-contact parts of the approach and retraction curves [34,35]. It was taken into account by the independent determination of the zero force level for the approach and retraction curves using corresponding non-contact regions. It should be noted that the indentation rate is slightly lower than the piezo speed (by ~10% for this experiment setup) due to the cantilever deflection at the post-contact region.

Both E_{app} and E_{retr} increased with the piezo speed following a weak power law with exponents 0.064 ± 0.003, and 0.11 ± 0.01, respectively (Fig. 2A). The ratio E_{app}/E_{retr} also increased from ≈0.95 to ≈1.15; it was ≈1 at speeds 1–2 μm/s. The indentation rate dependence of F_{ad} on approach and retraction curves was opposite (Figs. 2B and S6). While F_{ad} on approach curves gradually decreased with piezo speed to near zero value at piezo speed 32 μm/s, F_{ad} on retraction curves had a local minimum at 1–2 μm/s speed and then increased. Jump-to-contact occurs when the force gradient exceeds the stiffness of the cantilever, so the probe and the compliant sample bulge toward each other. But at higher piezo speed

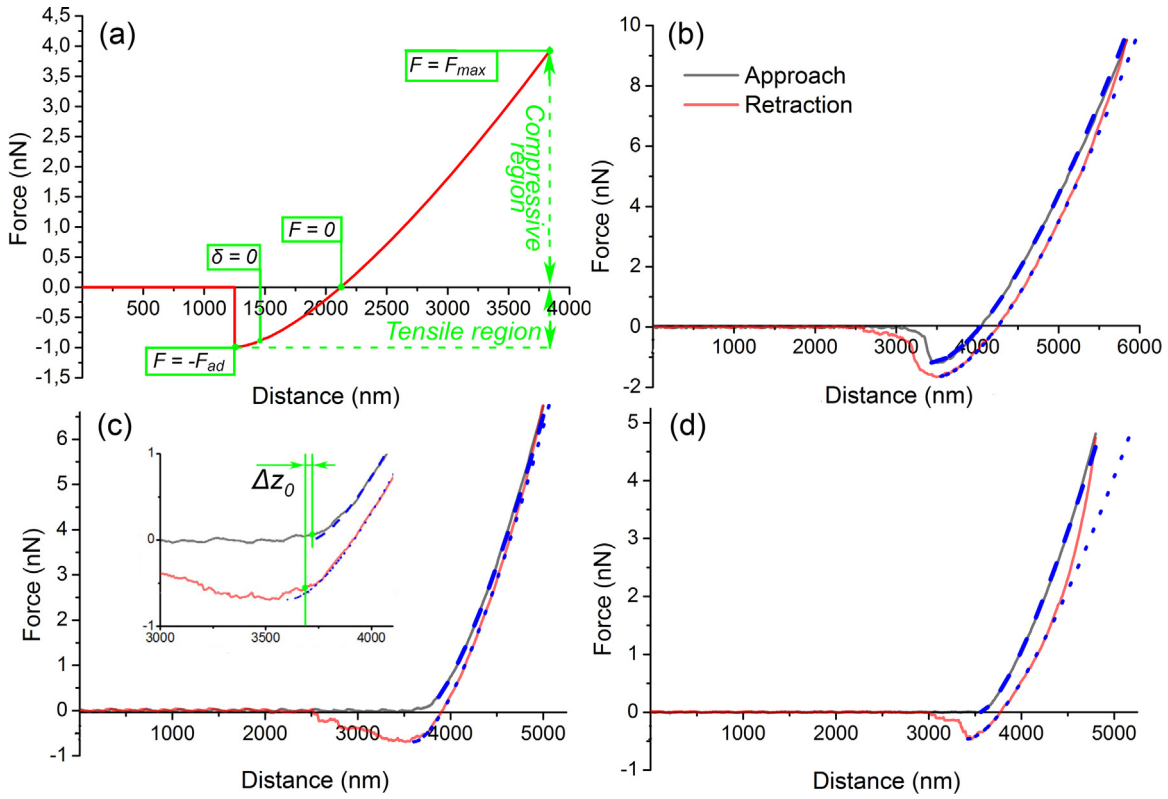

Fig. 1. Computed force curve following the JKR model (A) and experimental FCs from the PAA gels in water (B), PBS (C) and from Vero cell (D). The special points on computed curve are maximum load (F_{max}), maximum adhesion force (F_{ad}), zero load ($F=0$), zero displacement (z_0, $\delta=0$). Approach (black line) and retraction (red line) parts of FC and corresponding fits (dashed and dotted lines) are presented on the experimental curves. The insert shows the Δz_0 parameter determination. (For interpretation of the references to color in this figure legend, the reader is referred to the web version of this article.)

this effect does not appear due to the system inertia, and F_{ad} on approach curves decreases or vanishes. It seems that two opposite effects are manifested in the retraction curves. Low indentation rates led to prolonged contact time and higher work of adhesion γ, while high indentation rates also resulted in higher γ values because of the viscoelastic losses at the probe-sample interface, as will be discussed later. The work of detachment was proportional to F_{ad} and exposed the same behavior in all experiments (data not shown). The parameter Δz_0 had a local maximum at a piezo speed of near 10 μm/s (Fig. 2C). Apparently, it is affected by both the sample relaxation and the adhesion strength. The high adhesion force resulted in strong deformation and overextension of the sample, so measured Δz_0 values could be low and even negative. With an increase in the indentation rate, the relaxation processes led to the incomplete recovery of the sample during the probe retraction, so Δz_0 values increased. Then, at higher indentation rates, the growth of the adhesion force again could cause the decrease in Δz_0 values. At medium indentation rates and adhesion forces, Δz_0 is close to zero.

In order to investigate the influence of the holding time on the studied parameters, we varied the time of the probe-sample contact between approach and retraction from 0 to 10 s by maintaining the piezo displacement at a constant value. This experiment was carried out at a fixed indentation rate and maximum loading force F_{max} (2 μm/s and 9 nN, respectively). An increase in the holding time led to higher F_{ad} values on the retraction curves (Figs. 3A, S7). It is known that the adhesion force may increase with the holding time, probably due to the relaxation of stresses stored in asperities at the probe-sample contact, or due to the breakage of adsorbed layers of water molecules and ions between surfaces [36]. This fact can be interpreted as an increase of γ over contact time to its equilibrium value.

The force decay, which is caused by the gel relaxation, was measured as a relative (in percent) decrease in the maximum probe-sample interaction force after the holding period. It increased during the first 5 s of holding and was less than 10% for PAA gels (Figs. 3B, S7, S8). The ratio E_{app}/E_{retr} was close to one and nearly constant. The gel relaxation led to a decrease in the cantilever deflection and a corresponding increase in the indentation depth and contact area during holding, but it is quite small (≈1% change in contact area per 10 s holding time) and so could be neglected.

The maximum adhesion force F_{ad} on the retraction curves increased gradually with the indentation depth (and, accordingly, maximum load), while the other parameters were nearly constant (Figs. 3C and S9). This fact can be explained by the elevated contact time for the deeper indentations with a constant piezo speed.

3.2. PAA gels in PBS

The jump-to-contact was not observed during indentations at the piezo speeds used, so here the Hertz model was employed for approach curve processing ($|F_{ad}/F_{max}| \approx 0$). However, adhesion was presented during retraction, so the JKR model was used for retraction curve processing ($|F_{ad}/F_{max}| > 0.05$). The charges of the probe and gel surfaces in PBS (pH 7.4) and in water (pH ~6) should be similar. Apparently, the high ionic strength of a PBS solution (162.7 mM, Debye length ≈0.76 nm) decreases drastically the range of electrostatic attractive forces required for the jump-to-contact. Similarly, there was no detectable electrostatic interaction in PBS between the colloid probe and bare glass (Fig. S2). High ionic strength could also decrease the Hamaker constant and strength of van der Waals interactions [37]. These facts may also explain the ≈30% lower F_{ad} values observed on the retraction curves (at piezo speed 2 μm/s). In general, the behavior of the parameters E_{app}, E_{retr}, E_{app}/E_{retr}, Δz_0,

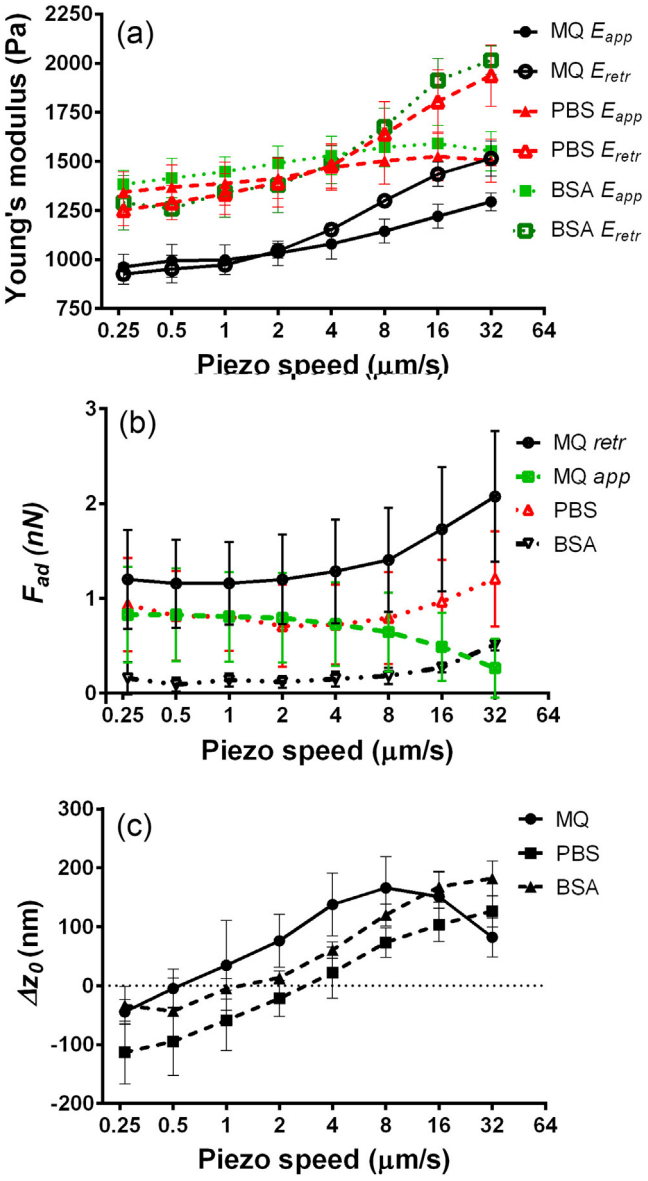

Fig. 2. Variation of the F_{ad} (A), E_{app} and E_{retr} (B), Δz_0 (C) with the piezo speed for PAA gels in MQ water, PBS, and PBS with 1% BSA. Error bars represent SD, $n = 3$.

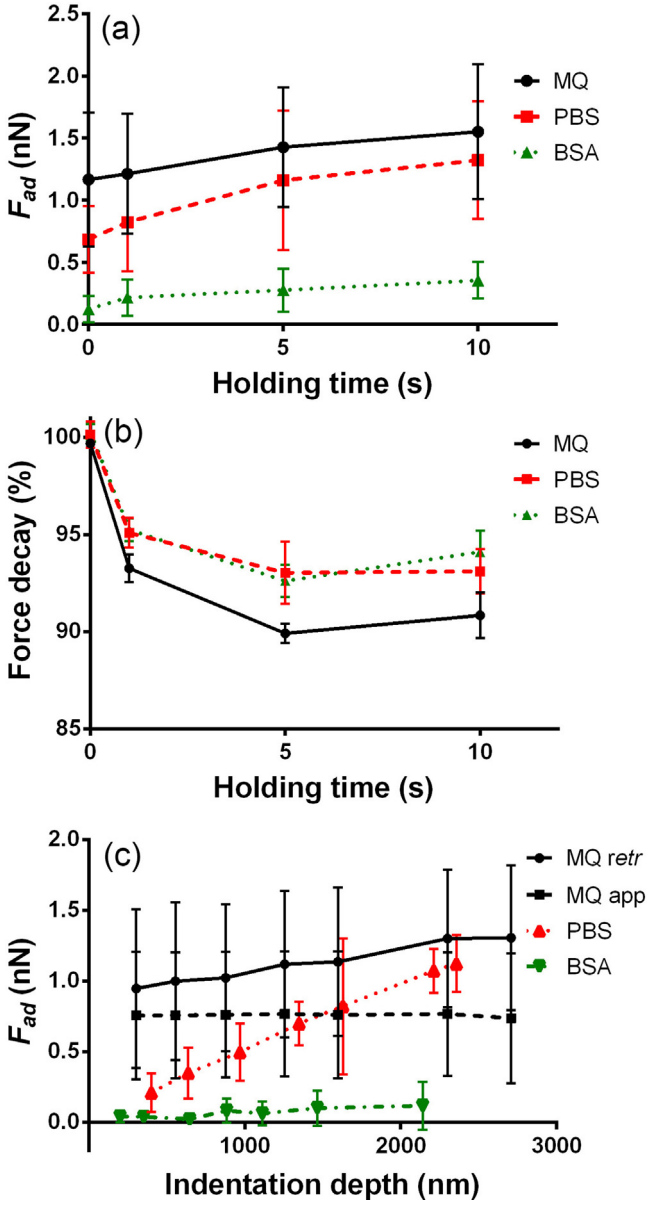

Fig. 3. Variation of the F_{ad} (A), and force decay (B) with holding time; variation of the F_{ad} with indentation depth (C) for PAA gels in MQ water, PBS, and PBS with 1% BSA. Error bars represent SD, $n = 3$.

F_{ad} was close to that in the experiments with different piezo speeds, holding times and indentation depths for the PAA gels in MQ water (Figs. 2 and 3). However, 40% higher E_{app} (1420 ± 90 Pa) and E_{retr} (1400 ± 100 Pa) values were observed, possibly due to different swelling of the PAA gels in the presence of salts [38]. These values are in good agreement with the Young's modulus E measured by the rheometer for the PAA gels in PBS (1300 ± 250 Pa). The exponents in the power law for the PAA gels in PBS were the same for E_{retr} and twice as low for E_{app} compared to the gels in MQ water, possibly due to the gel stiffening. For the same reason, the force decay was almost twice as low for the gels in PBS (Fig. 3B).

To reduce the non-specific interactions, 1% BSA was added into PBS prior to the measurements. After that, the measured F_{ad} values were about 0.1–0.2 nN, which is 4–7 times lower than the values for PAA gels in the absence of BSA (Fig. S5). Here the Hertz model could be applied to retraction curves ($|F_{ad}/F_{max}| < 0.05$, since F_{max} was ≈5–10 nN). The application of the JKR and Hertz models gave almost the same E values for such curves. BSA addition eliminates the hysteresis in the FCs caused by adhesion while the hysteresis caused by bulk viscoelastic behavior is preserved (Figs. S6, S7, S9). Accordingly, no differences were observed in the E_{app}, E_{retr} and force decay dependencies on loading rates, holding time and indentation depth for gels in PBS with and without BSA (Figs. 2 and 3).

3.3. *Vero cells in L-15 medium*

The measurement of the mechanical properties of cells and gels is generally similar, but there are certain differences as observed in the experiments. As in the case of PAA gels in PBS, the jump-to-contact was absent during cell indentations, so the Hertz model was employed for the processing of the approach curves. Cell mediums, including L15 medium (pH 7.4), typically have a high ionic strength comparable to that of PBS, which is required for the cell viability. Thus, the long-range electrostatic interactions are mainly screened. Unlike the PAA gels, cells demonstrated huge variability (CoV ≈70–90%) in Young's moduli and F_{ad}. Distributions of both parameters in cell population were wide and close to log-normal (Fig. 4A,B), which may be an inherent cell property and was demon-

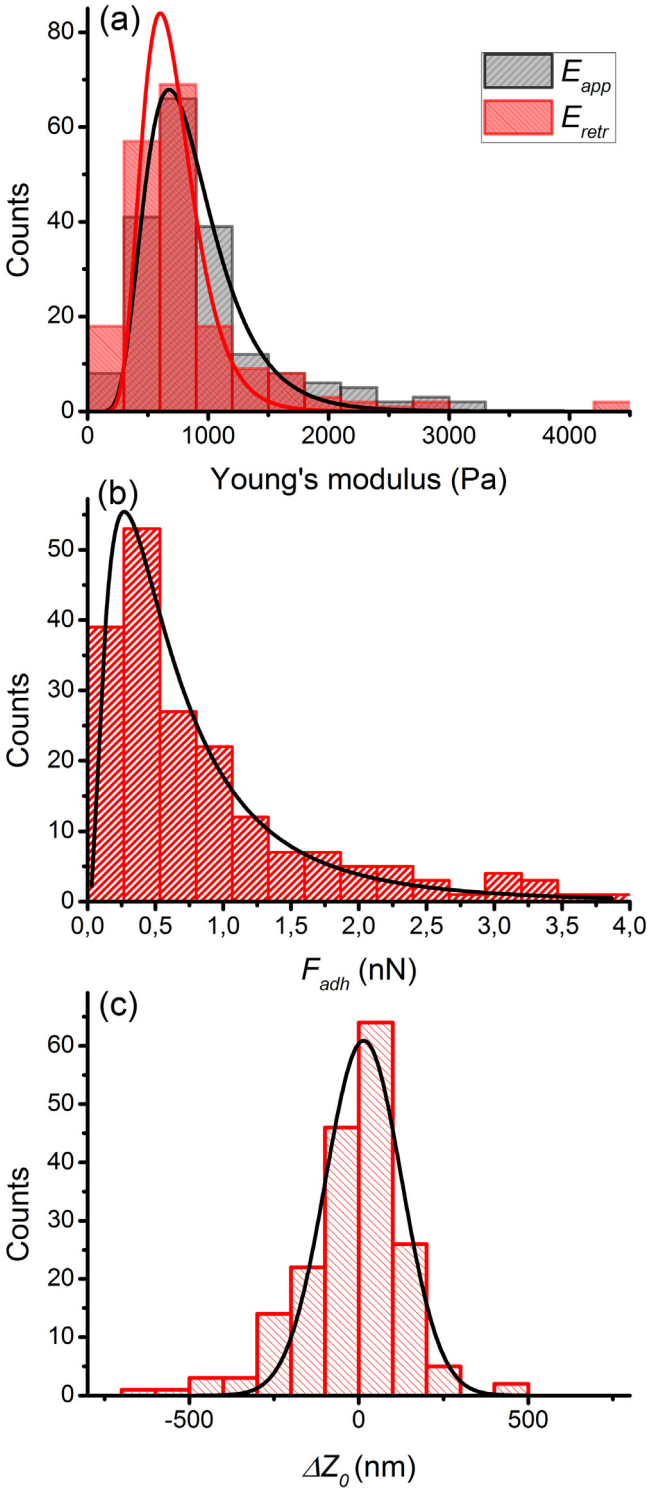

Fig. 4. Distributions of E_{app} and E_{retr} (A), F_{ad} (B), and Δz_0 (C) of Vero cells at 2 μm/s piezo speed. Solid lines represent log-normal (E_{app}, E_{retr}, F_{ad}) and normal (Δz_0) distribution function fit.

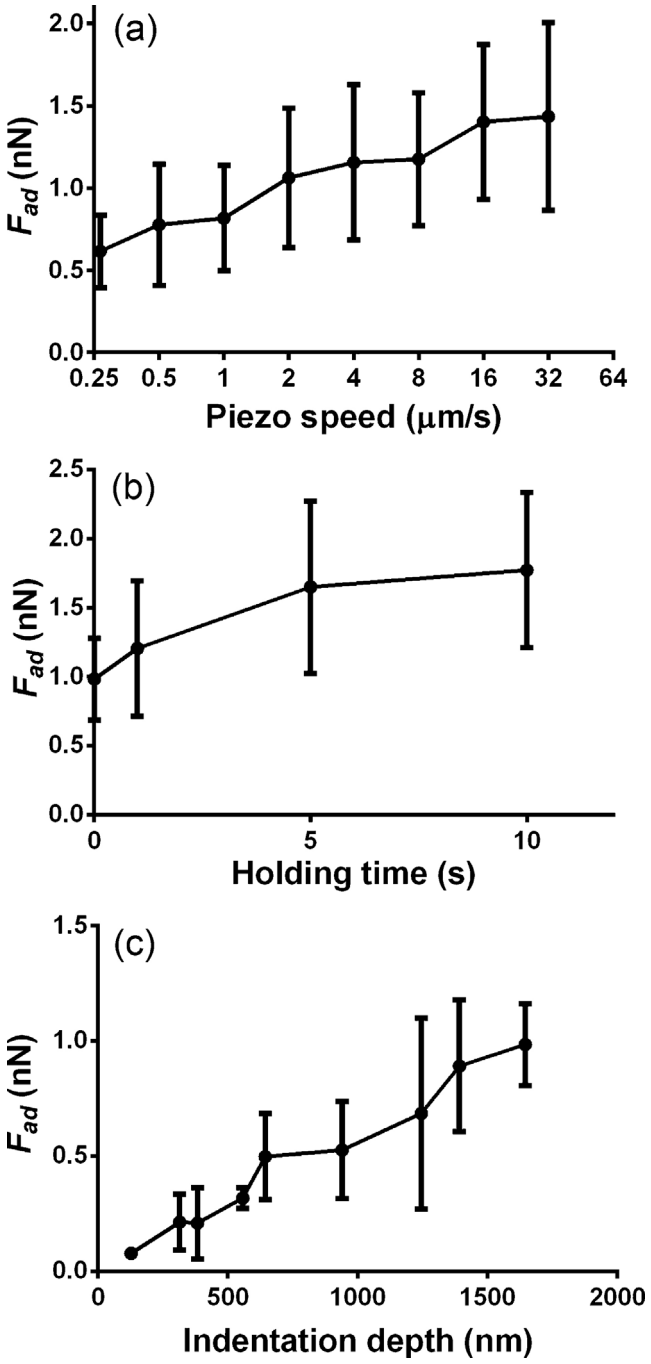

Fig. 5. Variation of the maximum adhesion force between the colloidal probe and Vero cells F_{ad} with the indentation rate (A), contact time (B) and indentation depth (C). Error bars represent SD, $n = 5$.

strated in other studies on cells [24,39,40]. At the same time, Δz_0 parameter distribution was close to Gaussian with a center near zero (Fig. 4C). No correlation between E_{app} (or E_{retr}) and F_{ad} was found (Spearman rank test coefficient, $r = -0.031$; $p = 0.605$), but significant negative correlation between F_{ad} and Δz_0 was observed ($r = -0.466$; $p = 0.0001$).

The adhesion force F_{ad} increased with the indentation rate, holding time and indentation depth (Figs. 5, S6–9). Young's modulus increased with piezo speed following a weak power law with exponents 0.1 for E_{app} and 0.17 for E_{retr} (Fig. 6A), which is higher than for the PAA gels. The Δz_0 parameter behaved in the same way as in the experiments with PAA gels: it had a zero value at low piezo speeds and then increased (Fig. 6B).

Cells demonstrated more viscous behavior than the PAA gels. The force decay per 10 s achieved 30–40% (Fig. 6C). Indeed, for the PAA gels, force relaxation can be roughly described by single exponential decay in accordance with the standard linear solid model [41], while for cells the power law decay model is more appropriate [9,42,43]. The associated increase in the indentation depth and

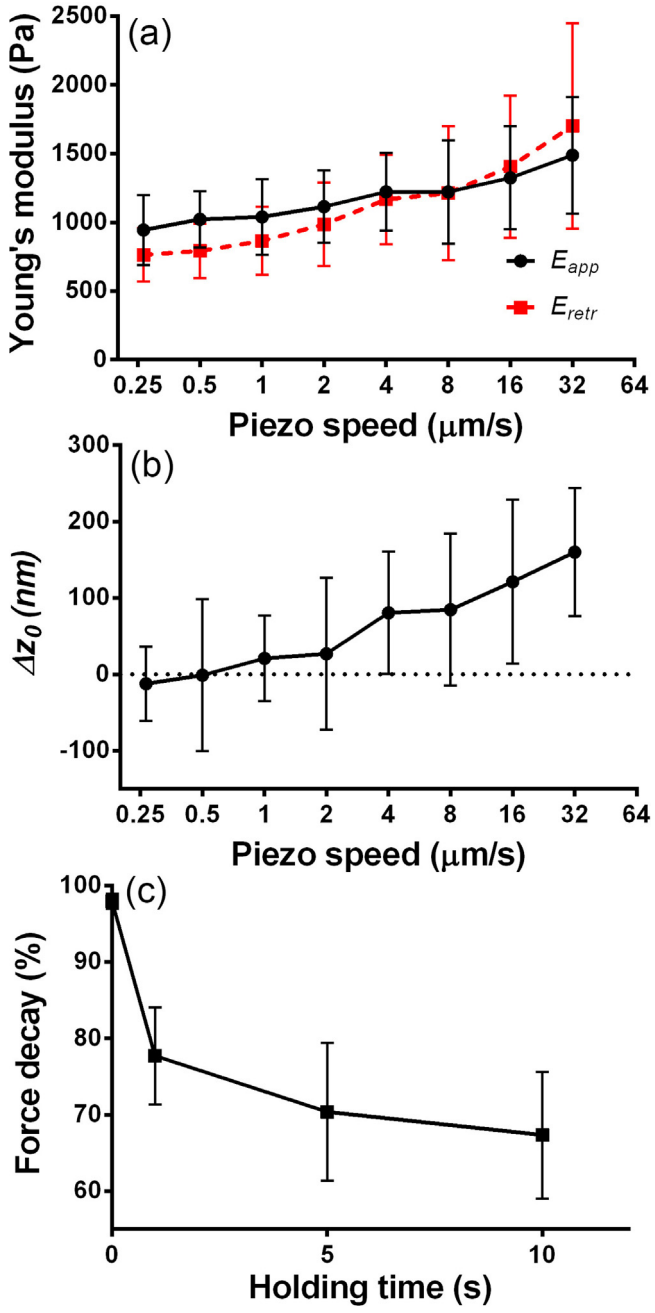

Fig. 6. Experiments on Vero cells in the L15 medium. Dependencies of E_{app}, E_{retr} (A) and Δz_0 (B) from the indentation rate. Dependence of the force decay from the holding time (C). Error bars represent SD, $n = 5$.

contact area due to the decrease in cantilever deflection achieved ≈6%, which may contribute to the increase in F_{ad}.

Contrary to the case of the PAA gels, the addition of 1% BSA to the cell medium led to a significant (3–4 fold) increase in F_{ad}. Accordingly, a decrease in Δz_0 was observed. Otherwise, the functional form of the experimental dependencies did not change (Fig. S10). The BSA concentration used (1%) is on the same order as the total protein concentration in a complete cell medium (with 10% FBS).

4. Discussion

The retraction portion of FC contains information about both the viscoelastic and adhesive properties of the material, but proper models should be applied for data extraction. Among the models that take adhesion into account, the JKR model seems to be the most suitable for the majority of AFM experiments with colloidal probes and soft samples like cells. Here, the applicability of the JKR model was tested on the PAA gels and Vero cells under different experimental conditions. In general, the retraction curves fitted well with the JKR model equation (Adjusted R-Squared ≈0.9–0.99). However, instabilities in the tensile part of the curve and relaxation at the upper part sometimes led to poor fit quality. The instabilities in the tensile part may be caused by surface roughness [32], and membrane–cytoskeleton detachment in the case of cells, while the compressive part should be less affected by these factors. Therefore, here we used only the compression part of the retraction curves for fitting.

The sample relaxation led to the violation of the JKR model assumptions. This effect was especially significant at the upper part of the retraction curves (Fig. 1D). Thus, processing of the whole retraction curve will lead to huge overestimation of Young's modulus [22]. Therefore, here we excluded the upper part of the curve and used only the first 750 nm of indentation for the PAA gels and 500 nm for Vero cells in the fitting procedure. This confinement also helped to exclude the abnormalities associated with the finite probe radius (the JKR model assumes $a \ll R$, which is violated at high indentation) and finite sample thickness. The applicability of the JKR model fit for processing the mid-range of the force curves was shown in other works for elastomeric samples [32,44].

The two parameters were introduced for the comparison of data obtained from the approach and retraction curves: the ratio E_{app}/E_{retr} and the difference between zero indentation points during approach and retraction Δz_0. At 2 μm/s piezo speed (the typical piezo speed used here) the ratio E_{app}/E_{retr} was close to 1 and Δz_0 was close to 0, which proves the applicability of the JKR model (Figs. 2 A,C and 6 A,B).

Growth of the F_{ad} with the indentation rate can be explained in the context of fracture mechanics [45–47]. In fracture mechanics terminology, the contact line is commonly viewed as a crack. The effective work of adhesion done while separating two surfaces is a function of the crack propagation rate, which is in turn affected by the local interfacial viscoelasticity. While the JKR model considers the thermodynamic equilibrium case, in real experiments the viscoelastic losses at the probe-sample interface lead to an increase in the effective work of adhesion with indentation speed. Accordingly, an increase in F_{ad} is observed on experimental FCs (Figs. 2B and 5B). The kinetics of adherence of viscoelastic bodies is now under theoretical and experimental study, and a good correspondence between theory and experiments was obtained for such elastomer as poly(dimethylsiloxane) [36,48,49]. However, cells with complex internal structure (membrane, cytoskeleton, and cytoplasm) represent a more complicated case. And while the general trend in F_{ad} dependence is preserved, further investigations are needed to clarify the applicability of the existing models. For example, it was shown that for cells, growth of the F_{ad} with the indentation rate may be observed if cell-to-probe adhesion is mediated by receptor-ligand binding with a high receptor-ligand reaction rate [50].

Parameters E_{app}, E_{retr} and Δz_0 are indentation rate-dependent; this reflects the shortcomings of the Hertz and JKR models, which do not take the viscous properties of the sample into account. The growth of E_{app} and E_{retr} and the hysteresis between approach/retraction curves (E_{app}/E_{retr} ratio) with indentation rate (Fig. S6) is caused by the bulk viscoelasticity of the PAA gel samples and Vero cells and is less affected by adhesion. Indeed, when the adhesion force on gel samples was diminished by the BSA addition, the form of indentation rate dependencies of E_{app} and E_{retr} was preserved (Fig. 2A). It was also preserved for cells with medium and high (after BSA addition) adhesion. The power law rate dependencies of E_{app} and E_{retr} were observed previously, and exponents for E_{app} for cells are in the range of 0.1–0.3 [24,51,52].

Several rheology experiments on cells have also shown that the frequency dependent stiffness of the cells follows a weak power law [24,52,53].

Relaxation and creep take place during the indentation cycle and affect the contact area, so the shape of the approach and retraction curves is modified and the Hertz/JKR model assumptions are violated. If the functional form of the relaxation is known then the stress relaxation and creep compliance can be extracted from one set of indentation data (whole FC) with proper equations, and both the Hertz and the JKR models should be modified accordingly. Otherwise, parameter Δz_0, E_{app}/E_{retr} and the force decay at the chosen indentation rate and holding time can be used for the qualitative evaluation of viscoelastic properties. Here, the more viscous behavior of cells was manifested in elevated values of the force decay and higher exponent values in E_{app} and E_{retr} dependencies from indentation rate than in corresponding values for the PAA gels. The entire force–time decay curves (Fig. S8) can be processed to extract more detailed relaxational responses [27,54]. Parameter Δz_0 is affected by both bulk viscous properties and the adhesion forces, so its behavior is rather difficult to interpret. It could be used to determine plasticity (the force-induced irreversible deformation) of the sample. Here we did not observe plasticity for either PAA gels or Vero cells, since the position of the contact point is preserved for the FCs recorded within several seconds after the previous measurement.

The adhesion forces between the cell or PAA gel and probe may have different origins, including electrostatic, van der Waals, hydrogen bonding and others [55]. All of them may contribute to the work of adhesion and to its change with the time of contact. Since both cell and probe surfaces are charged negatively at neutral pH (cell due to sialic acid residues of glycoproteins and glycolipids located at the cell surface in the glycocalyx layer [56]), the possibility of electrostatic bonds was low and electrostatic repulsion could arise. Electrostatic forces have a more significant effect in MQ water, and are mostly screened in PBS and cell medium due to high ionic strength. Long-range electrostatic attraction between the probe and PAA gel was observed in MQ water. It could be handled as suggested in [57] for the case of non-contact repulsion. The long-range repulsive (or attractive) force is assumed to reach a maximum value at the point of contact and then be constant throughout the indentation cycle. Consequently, the force curve in the contact region is simply offset by a distance corresponding to the maximum repulsive force, which has no effect on the elastic response of the sample. A similar approach can be used for the treatment of attractive forces. In that case, the measured F_{ad} value is the sum of long-range attractive forces and short-range adhesion forces, while measured E values should not be affected.

Growth of F_{ad} with holding time can be explained by the non-equilibrium conditions in the sample-probe system. After sample-probe contact is established, the work of adhesion γ increases to its equilibrium value, probably due to the relaxation of stresses stored in asperities at the probe-sample contact or due to the breakage of adsorbed layers of water molecules and ions between surfaces [36]. For cells, the equilibrium, if actually possible, can only be achieved on a very long timescale. It was shown, that growth in F_{ad} value occurs even at 60 min holding time [58]. It is explained with the ability of cells to build specific protein contacts with the probe surface.

Since the adhesion between the sample and the probe only develops over time, it is an interesting question to determine when exactly Hertzian contact turns into JKR contact, and whether adhesion could affect approach curves (E_{app}) or not in case when jump-to-contact is not presented. According to our data, the adhesion did not affect the measured E_{app} values: in experiments with PAA gels we did not observe significant changes in E_{app} (and also E_{retr}) before and after BSA addition, which led to a significant decrease in adhesion force. Also, in experiments with cells, no correlation between E_{app} and F_{ad} were found. Moreover, BSA addition, which causes an increase in adhesion force, did not lead to the significant alteration of E_{app} values. It seems that the contact area follows the Hertz model during the approach, if jump-to-contact is not observed. Without long-range forces, the adhesion bonds are formed only inside the Hertz contact area. And when retraction starts, the contact begins to follow the JKR model due to the presence of the adhesion. However, the transition from Hertzian to JKR contact is complicated due to sample bulk and interfacial viscoelasticity (relaxation and crack propagation).

Adhesion forces between the probe and sample can be reduced by different ways. For example, detergent can be added to the medium to eliminate interfacial forces [44]. Here, the addition of 1% BSA solution greatly lowered adhesion between the probe and PAA gels due to BSA's ability to block the hydrophobic and charged binding sites on the surfaces (Fig. S5). However, the adhesivity of Vero cells increased in the presence of BSA. The above results show that presence of proteins in the medium also affects probe-cell adhesion, which may be connected with endocytosis-associated or receptor-ligand binding events on the cell surface. It was shown that probe hydrophobization can decrease adhesion to the cell surface [9], but not completely, and this effect can be cell specific [59]. Overall, cell adhesion is a very specific matter and can be affected by cell type, probe material, medium composition and other parameters.

5. Conclusions

The indentation rate, depth and holding time dependencies of adhesion forces indicate that AFM indentation experiments on gels and cells are performed under non-equilibrium conditions. Both bulk and local interfacial viscoelasticity can affect the measurements. In the AFM experiments with cells, the tip-sample equilibrium is elusive due to the complicated nature of the surface interactions, including protein-bond formation and endocytosis. Still, the JKR model fits the retraction part of FCs acquired at medium indentation rates (1–8 μm/s) and low holding times (up to 10 s) well enough to extract data about the mechanical properties of the samples, including maximum adhesion force, Young's moduli and the point of zero indentation. A comparison of these parameters with the data from the approach part of FCs may allow the assessment of viscoelastic properties of the sample.

The observed maximum adhesion force depends on the probe-sample contact time and loading rate. A higher contact time and loading rate lead to an increase in adhesion due to the complex nature of the probe-sample contact. The medium composition (ionic strength, presence of proteins) also impacted the adhesion force by regulating the probe-sample interaction.

Acknowledgements

This work has been partially supported by the RFBR grant 13-04-01570 a. The authors thank D.D. Khaydapova and E.Yu. Milanovskiy for the help in performing experiments on the rheometer.

Appendix A. Supplementary data

Supplementary data associated with this article can be found, in the online version, at http://dx.doi.org/10.1016/j.colsurfb.2015.06.044001

References

[1] C. Rotsch, M. Radmacher, Drug-induced changes of cytoskeletal structure and mechanics in fibroblasts: an atomic force microscopy study, Biophys. J. 78 (2000) 520–535.
[2] M. Flores-Merino, S. Chirasatitsin, Nanoscopic mechanical anisotropy in hydrogel surfaces, Soft Matter. 6 (2010) 4466–4470.
[3] A.J. Engler, L. Richert, J.Y. Wong, C. Picart, D.E. Discher, Surface probe measurements of the elasticity of sectioned tissue, thin gels and polyelectrolyte multilayer films: correlations between substrate stiffness and cell adhesion, Surf. Sci. 570 (2004) 142–154.
[4] T.G. Kuznetsova, M.N. Starodubtseva, N.I. Yegorenkov, S.A. Chizhik, R.I. Zhdanov, Atomic force microscopy probing of cell elasticity, Micron 38 (2007) 824–833.
[5] E.K. Dimitriadis, F. Horkay, J. Maresca, B. Kachar, R.S. Chadwick, Determination of elastic moduli of thin layers of soft material using the atomic force microscope, Biophys. J. 82 (2002) 2798–2810.
[6] L. Sirghi, Atomic force microscopy indentation of living cells, Microsc. Sci. Technol. Appl. Educ. 4 (2010) 433–440.
[7] M. Kappl, H.-J. Butt, The colloidal probe technique and its application to adhesion force measurements, Part. Part. Syst. Charact. 19 (2002) 129–143.
[8] Y. Sun, B. Akhremitchev, G. Walker, Using the adhesive interaction between atomic force microscopy tips and polymer surfaces to measure the elastic modulus of compliant samples, Langmuir 20 (2004) 5837–5845.
[9] S. Hiratsuka, Y. Mizutani, A. Toda, N. Fukushima, K. Kawahara, H. Tokumoto, et al., Power-law stress and creep relaxations of single cells measured by colloidal probe atomic force microscopy, Jpn. J. Appl. Phys. 48 (2009) 08JB17.
[10] Y.M. Efremov, D.V. Bagrov, E.V. Dubrovin, K.V. Shaitan, I.V. Yaminskii, Atomic force microscopy of animal cells: advances and prospects, Biophysics 56 (2011) 257–267.
[11] K. Haase, A.E. Pelling, Investigating cell mechanics with atomic force microscopy, J. R. Soc. Interface. 12 (2015) 20140970.
[12] K.A. Melzak, S. Moreno-Flores, A.E. López, J.L. Toca-Herrera, Why size and speed matter: frequency dependence and the mechanical properties of biomolecules, Soft Matter 7 (2011) 332–342.
[13] M. Lekka, K. Pogoda, J. Gostek, O. Klymenko, S. Prauzner-Bechcicki, J. Wiltowska-Zuber, et al., Cancer cell recognition–mechanical phenotype, Micron 43 (2012) 1259–1266.
[14] Y.M. Efremov, M.E. Lomakina, D.V. Bagrov, P.I. Makhnovskiy, A.Y. Alexandrova, M.P. Kirpichnikov, et al., Mechanical properties of fibroblasts depend on level of cancer transformation, Biochim. Biophys. Acta 1843 (2014) 1013–1019.
[15] L.M. Rebelo, J.S. de Sousa, J. Mendes Filho, M. Radmacher, Comparison of the viscoelastic properties of cells from different kidney cancer phenotypes measured with atomic force microscopy, Nanotechnology 24 (2013) 055102.
[16] L. Sirghi, J. Ponti, F. Broggi, F. Rossi, Probing elasticity and adhesion of live cells by atomic force microscopy indentation, Eur. Biophys. J. 37 (2008) 935–945.
[17] D.C. Lin, E.K. Dimitriadis, F. Horkay, Robust strategies for automated AFM force curve analysis-II: adhesion-influenced indentation of soft, elastic materials, J. Biomech. Eng. 129 (2007) 904–912.
[18] C.E. McNamee, N. Pyo, S. Tanaka, I.U. Vakarelski, Y. Kanda, K. Higashitani, Parameters affecting the adhesion strength between a living cell and a colloid probe when measured by the atomic force microscope, Colloids Surf. B. Biointerfaces 48 (2006) 176–182.
[19] S.M. Wiederhorn, Y.-H. Chae, C.G. Simon, J. Cahn, Y. Deng, D. Day, Cell adhesion to borate glasses by colloidal probe microscopy, Acta Biomater. 7 (2011) 2256–2263.
[20] B. Codan, G. Del Favero, V. Martinelli, C.S. Long, L. Mestroni, O. Sbaizero, Exploring the elasticity and adhesion behavior of cardiac fibroblasts by atomic force microscopy indentation, Mater. Sci. Eng. C. Mater. Biol. Appl. 40 (2014) 427–434.
[21] A.B. Mathur, A.M. Collinsworth, W.M. Reichert, W.E. Kraus, G.A. Truskey, Endothelial, cardiac muscle and skeletal muscle exhibit different viscous and elastic properties as determined by atomic force microscopy, J. Biomech. 34 (2001) 1545–1553.
[22] M. Prabhune, G. Belge, A. Dotzauer, J. Bullerdiek, M. Radmacher, Comparison of mechanical properties of normal and malignant thyroid cells, Micron 43 (2012) 1267–1272.
[23] T. Boudou, J. Ohayon, C. Picart, P. Tracqui, An extended relationship for the characterization of Young's modulus and Poisson's ratio of tunable polyacrylamide gels, Biorheology 43 (2006) 721–728.
[24] Y.M. Efremov, A.A. Dokrunova, D.V. Bagrov, K.S. Kudryashova, O.S. Sokolova, K.V. Shaitan, The effects of confluency on cell mechanical properties, J. Biomech. 46 (2013) 1081–1087.
[25] H.-J. Butt, M. Jaschke, Calculation of thermal noise in atomic force microscopy, Nanotechnology 6 (1995) 1–7.
[26] J.E. Sader, J.W.M. Chon, P. Mulvaney, Calibration of rectangular atomic force microscope cantilevers, Rev. Sci. Instrum. 70 (1999) 3967–3969.
[27] S. Tripathy, E.J. Berger, Measuring viscoelasticity of soft samples using atomic force microscopy, J. Biomech. Eng. 131 (2009) 094507.
[28] K. Johnson, J. Greenwood, An adhesion map for the contact of elastic spheres, J. Colloid Interface. Sci. 192 (1997) 326–333.
[29] K. Johnson, K. Kendall, A. Roberts, Surface energy and the contact of elastic solids, Proc. R. Soc. Lond. 324 (1971) 301–313.
[30] D. Maugis, Adhesion of spheres: the JKR-DMT transition using a Dugdale model, J. Colloid Interface Sci. 150 (1992) 243–269.
[31] D. Tabor, Surface forces and surface interactions, J. Colloid Interface Sci. 58 (1977) 2–13.
[32] F.M. Borodich, B.A. Galanov, S.N. Gorb, M.Y. Prostov, Y.I. Prostov, M.M. Suarez-Alvarez, Evaluation of adhesive and elastic properties of materials by depth-sensing indentation of spheres, Appl. Phys. A 108 (2012) 13–18.
[33] P.G. Hartley, I. Larson, P.J. Scales, Electrokinetic and direct force measurements between silica and mica surfaces in dilute electrolyte solutions, Langmuir 13 (1997) 2207–2214.
[34] J.V. Méndez-Méndez, M.T. Alonso-Rasgado, E. Correia Faria, E.A. Flores-Johnson, R.D. Snook, Numerical study of the hydrodynamic drag force in atomic force microscopy measurements undertaken in fluids, Micron 66 (2014) 37–46.
[35] J. Janovjak, Hydrodynamic effects in fast AFM single-molecule force measurements, Eur. Biophys. J. 34 (2005) 91–96.
[36] I.U. Vakarelski, A. Toritani, M. Nakayama, K. Higashitani, Deformation and adhesion of elastomer microparticles evaluated by AFM, Langmuir 17 (2001) 4739–4745.
[37] F.L. Leite, C.C. Bueno, A.L. Da Róz, E.C. Ziemath, O.N. Oliveira, Theoretical models for surface forces and adhesion and their measurement using atomic force microscopy, Int. J. Mol. Sci. 13 (2012) 12773–12856.
[38] M. Sivanantham, B.V.R. Tata, Swelling/deswelling of polyacrylamide gels in aqueous NaCl solution: light scattering and macroscopic swelling study, Pramana–J. Phys. 79 (2012) 457–469.
[39] S. Hiratsuka, Y. Mizutani, M. Tsuchiya, K. Kawahara, H. Tokumoto, T. Okajima, The number distribution of complex shear modulus of single cells measured by atomic force microscopy, Ultramicroscopy 109 (2009) 937–941.
[40] A.N. Ketene, E.M. Schmelz, P.C. Roberts, M. Agah, The effects of cancer progression on the viscoelasticity of ovarian cell cytoskeleton structures, Nanomedicine 8 (2012) 93–102.
[41] M. Galli, K.S.C. Comley, T.A.V. Shean, M.L. Oyen, Viscoelastic and poroelastic mechanical characterization of hydrated gels, J. Mater. Res. 24 (2009) 973–979.
[42] P. Kollmannsberger, B. Fabry, Linear and nonlinear rheology of living cells, Annu. Rev. Mater. Res. 41 (2011) 75–97.
[43] N. Desprat, A. Richert, J. Simeon, A. Asnacios, Creep function of a single living cell, Biophys. J. 88 (2005) 2224–2233.
[44] D.M. Ebenstein, Nano-JKR force curve method overcomes challenges of surface detection and adhesion for nanoindentation of a compliant polymer in air and water, J. Mater. Res. 26 (2011) 1026–1035.
[45] D. Maugis, M. Barquins, Fracture mechanics and the adherence of viscoelastic bodies, J. Phys. D Appl. Phys. 11 (1978) 1989–2023.
[46] J.A. Greenwood, K.L. Johnson, The mechanics of adhesion of viscoelastic solids, Philos. Mag. A 43 (1981) 697–711.
[47] J.A. Greenwood, K.L. Johnson, Oscillatory loading of a viscoelastic adhesive contact, J. Colloid Interface Sci. 296 (2006) 284–291.
[48] R. Buzio, A. Bosca, S. Krol, D. Marchetto, S. Valeri, U. Valbusa, Deformation and adhesion of elastomer poly(dimethylsiloxane) colloidal AFM probes, Langmuir 23 (2007) 9293–9302.
[49] Y. Sun, G.C. Walker, Viscoelastic response of poly(dimethylsiloxane) in the adhesive interaction with AFM tips, Langmuir 21 (2005) 8694–8702.
[50] C.Y. Zhang, Y.W. Zhang, Computational analysis of adhesion force in the indentation of cells using atomic force microscopy, Phys. Rev. E Stat. Nonlin. Soft Matter. Phys. 77 (2008) 1–8.
[51] Q.S. Li, G.Y.H. Lee, C.N. Ong, C.T. Lim, AFM indentation study of breast cancer cells, Biochem. Biophys. Res. Commun. 374 (2008) 609–613.
[52] S. Nawaz, P. Sánchez, K. Bodensiek, S. Li, M. Simons, I.A.T. Schaap, Cell visco-elasticity measured with AFM and optical trapping at sub-micrometer deformations, PLoS One 7 (2012) e45297.
[53] B.D. Hoffman, J.C. Crocker, Cell mechanics: dissecting the physical responses of cells to force, Annu. Rev. Biomed. Eng. 11 (2009) 259–288.
[54] S. Moreno-Flores, R. Benitez, M.D. Vivanco, J.L. Toca-Herrera, Stress relaxation microscopy: imaging local stress in cells, J. Biomech. 43 (2010) 349–354.
[55] N. Pyo, S. Tanaka, C.E. McNamee, Y. Kanda, Y. Fukumori, H. Ichikawa, et al., Effect of the cell type and cell density on the binding of living cells to a silica particle: an atomic force microscope study, Colloids Surf. B Biointerfaces 53 (2006) 278–287.
[56] A. Alberts, J. Johnson, M. Lewis, K. Raff, Molecular Biology of the Cell, Chapter 10, Membrane Structure, 4th ed., Garland Science, New York, 2002, pp. 583–615.
[57] E. Lin, Advances in the mechanical characterization of soft materials by nanoindentation, in: S. Pandalai (Ed.), Recent Reserch Devlopment Biophysics, Transworld Research Network, Kerala, India, 2006, pp. 333–370.
[58] C.E. McNamee, N. Pyo, K. Higashitani, Atomic force microscopy study of the specific adhesion between a colloid particle and a living melanoma cell: effect of the charge and the hydrophobicity of the particle surface, Biophys. J. 91 (2006) 1960–1969.
[59] C.E. McNamee, Y. Aso, S. Yamamoto, Y. Fukumori, H. Ichikawa, K. Higashitani, Chemical groups that adhere to the surfaces of living malignant cells, Pharm. Res. 24 (2007) 2370–2380.